Research Article | Vol. 27, No. 6 | 18 Mar 2019 | OPTICS EXPRESS 8308
Optics EXPRESS

Analysis of modal coupling due to birefringence and ellipticity in strongly guiding ring-core OAM fibers

GIANLUCA GUERRA,[1,4] MATTEO LONARDI,[2] ANDREA GALTAROSSA,[1] LESLIE A. RUSCH,[3] ALBERTO BONONI[2] AND LUCA PALMIERI[1,5]

[1] *Department of Information Engineering, University of Padova, Italy*
[2] *Department of Engineering and Architecture, University of Parma, Italy*
[3] *Department of Electrical and Computer Engineering, Université Laval, Québec, Canada*
[4] *gianluca.guerra@phd.unipd.it*
[5] *luca.palmieri@unipd.it*

Abstract: After briefly recalling the issue of OAM mode purity in strongly-guiding ring-core fibers, this paper provides a methodology to calculate the coupling strength between OAM mode groups due to fiber perturbations. The cases of stress birefringence and core ellipticity are theoretically and numerically investigated. It is found that both perturbations produce the same coupling pattern among mode groups, although with different intensities. The consequence is that birefringence causes the highest modal crosstalk because it strongly couples groups with a lower propagation-constant mismatch. The power coupling to parasitic TE and TM modes is also quantified for both perturbations and is found to be non-negligible. Approximate modal crosstalk formulas valid for weakly-guiding multi-core fibers, but whose parameters are adapted to the present case of strongly guiding OAM fibers, are found to provide a reasonable fit to numerical results. Finally, the effect that modal coupling has on OAM transmission is assessed in terms of SNR penalty.

1. Introduction

Spatial division multiplexing, or SDM, can increase the carrying capacity of optical fibers. Researchers are investigating how we could use this capacity expansion to bring down the cost per bit of information. Integration of components such as multiplexers, transceivers and amplifiers will play an important part in reducing cost. However, the optical fiber will determine the distance supported and will impact the effort required to recover information, particularly when modal multiplexing is used to achieve SDM. This paper examines the impact of deformities in fibers supporting orbital angular momentum (OAM) modes, focusing on core ellipticity and stress induced birefringence.

The greatest source of impairments in systems using mode multiplexing in few mode fibers (FMF) comes from the cross-correlation (or crosstalk) induced when multiplexing and co-propagating spatial modes. Two broad strategies have emerged for dealing with this cross-correlation: the use of extensive multiple input, multiple output (MIMO) processing to undo the correlations [1], and the use of components and fibers that avoid the introduction of correlations [2]. Each strategy has its advantages and disadvantages, and there is a lack of extensive modeling to quantify these differences. The distance that can be propagated before either strategy breaks down is of particular importance. MIMO processing can become prohibitively complex if the equalizer length grows linearly with distance. Thus research focuses on differential group delay in systems using MIMO [3]. Avoiding MIMO processing is only possible for distances where cross-correlations remain tolerable despite the effects of accumulated imperfections in the fiber. Hence, for systems targeting limited or no MIMO processing, research must address the source

#349416 https://doi.org/10.1364/OE.27.008308
Journal © 2019 Received 29 Oct 2018; revised 20 Dec 2018; accepted 27 Dec 2018; published 7 Mar 2019

Optics EXPRESS

and intensity of coupling between modes. This paper address the latter, i.e., systems avoiding extensive MIMO processing.

Reduced MIMO processing is possible for mode group multiplexing and for fibers designed to support modes with limited coupling. As capacity increase is greatest when exploiting individual modes (rather than mode groups) to carry data, we focus on systems that exploit both polarization multiplexing and individual mode multiplexing. Fibers supporting two types of modes have emerged for this kind of system: linearly polarized vector modes [4] and orbital angular momentum modes [5]. The linearly polarized vector (LPV) modes can be completely polarization maintaining or mix only in polarization; they do not mix in spatial modes. Both vector modes (LPV and OAM) have by their nature degenerate modes that come in pairs. Hence their MIMO complexity is capped at 2×2 MIMO elements, akin or equivalent to the 2×2 MIMO used commonly in polarization multiplexed systems today. The coupling of these pairs of degenerate modes would eventually require larger MIMO blocks [6]; strong coupling between all degenerate pairs would require extensive MIMO used with multiplexing of scalar modes. While some experimental effort has been made to identify coupling levels of OAM in different lengths of conventional fiber [7], we seek to model the coupling by applying multimode fibers techniques [8] to fibers with very high contrast refractive indices designed to support many OAM orders [9].

Expanding preliminary results presented in [10], we examine the source of coupling between OAM modes in fibers designed specifically to support their propagation. Previous modeling of the common coupling sources, core ellipticity and stress induced birefringence, must be adapted to the unusual nature of OAM degenerate modes. We start in Section 2 with an examination of the intrinsic presence of small modal impurities in OAM guided modes, and in Section 3 explain how this determines the number of coupling mechanisms. In Section 4 we move on to our numerical analysis of coupling for mode profiles from a specific OAM fiber design [9], assessing the effect of coupling in OAM transmission. We present results for various levels of perturbations and beat lengths. The last section offers some concluding remarks.

2. Modes of ring-core fibers

In an optical fiber made of R concentric homogeneous rings, the propagating field can be expanded in the eigenmodes basis $\mathrm{TE}_{0,p}$, $\mathrm{TM}_{0,p}$, $\mathrm{HE}_{\upsilon,p}$ and $\mathrm{EH}_{\upsilon,p}$, where υ and p are positive integers giving the mode azimuth order and counting for the specific solution, respectively [11]. Given the fiber circular symmetry, hybrid modes $\mathrm{HE}_{\upsilon,p}$ and $\mathrm{EH}_{\upsilon,p}$ come with a 2-fold degeneracy, even and odd. Letting $\mathbf{E}$ refer to either HE or EH modes, they can be written, with respect to cylindrical coordinates (r, φ), as [11]

$$\mathbf{E}_{\upsilon}^{\{\mathrm{e}\atop\mathrm{o}}(r,\varphi) = f_{\upsilon}(r) \cdot \begin{Bmatrix}\cos(\upsilon\varphi)\\ \sin(\upsilon\varphi)\end{Bmatrix} \hat{\mathbf{r}} + g_{\upsilon}(r) \cdot \begin{Bmatrix}\sin(\upsilon\varphi)\\ -\cos(\upsilon\varphi)\end{Bmatrix} \hat{\boldsymbol{\varphi}} + j h_{\upsilon}(r) \cdot \begin{Bmatrix}\cos(\upsilon\varphi)\\ \sin(\upsilon\varphi)\end{Bmatrix} \hat{\mathbf{z}}, \tag{1}$$

where f_{υ}, g_{υ} and h_{υ} are mode-dependent real functions and the upper index of $\mathbf{E}_{\upsilon}$ selects the even (e) or odd (o) degeneracy. We omit writing explicitly the counting index p for the sake of brevity.

An equivalent representation consists in combining even and odd degeneracies, which has the effect of producing helical phase fronts. This is achieved by simply defining the new HE and EH modes as $\mathbf{E}_{\pm\upsilon} \triangleq \mathbf{E}_{\upsilon}^{\mathrm{e}} \pm j\mathbf{E}_{\upsilon}^{\mathrm{o}}$, where the "+" and "−" choices produce left- and right-handed helical phase-fronts, respectively. The corresponding field expressions are

$$\begin{aligned}\mathbf{E}_{\pm\upsilon}(r,\varphi) =& \frac{1}{\sqrt{2}}[f_{\upsilon}(r) \pm g_{\upsilon}(r)] \exp\left[\pm j(\upsilon \mp 1)\varphi\right] \hat{\mathbf{L}} + \frac{1}{\sqrt{2}}[f_{\upsilon}(r) \mp g_{\upsilon}(r)] \exp\left[\pm j(\upsilon \pm 1)\varphi\right] \hat{\mathbf{R}} \\ &+ j h_{\upsilon}(r) \exp\left(\pm j\upsilon\varphi\right) \hat{\mathbf{z}},\end{aligned} \tag{2}$$

Optics EXPRESS

where the new circular polarization basis vectors $\hat{\mathbf{L}} = (\hat{\mathbf{r}} + j\hat{\boldsymbol{\varphi}})\exp(j\varphi)/\sqrt{2}$ and $\hat{\mathbf{R}} = (\hat{\mathbf{r}} - j\hat{\boldsymbol{\varphi}})\exp(-j\varphi)/\sqrt{2}$ are the left-handed circular polarization (LCP) state and the right-handed circular polarization (RCP) state, respectively. Equation (2) highlights that the LCP and RCP components are helical beams with the same handedness, but different orbital angular momentum (OAM) orders: either $\upsilon + 1$ or $\upsilon - 1$ [12, 13]. In weakly-guiding fibers, only one of the LCP and the RCP components survives, while the other is weak and almost negligible [14]; we call these two components dominant and secondary, respectively [15]. A simple way to determine which is the dominant component consists in noticing that weakly-guiding fibers are well described by the linearly polarized $\mathrm{LP}_{n,p}$ modes, whose transverse field components have azimuthal order n [11]. The $\mathrm{LP}_{n,p}$ modes are linear combinations of $\mathrm{HE}_{\pm(n+1),p}$ and $\mathrm{EH}_{\pm(n-1),p}$, for $n \neq 1$, or combinations of $\mathrm{HE}_{\pm 2,p}$, $\mathrm{TE}_{0,p}$ and $\mathrm{TM}_{0,p}$, for $n = 1$. Therefore, the dominant component is the one of order $\upsilon - 1$ for $\mathrm{HE}_{\upsilon,p}$ modes and of order $\upsilon + 1$ for the $\mathrm{EH}_{\upsilon,p}$ modes. The longitudinal component of the modes becomes almost negligible and the corresponding fields can be considered paraxial [11].

Traditionally, the OAM modes are defined as [2]

$$\mathrm{OAM}^{\pm}_{\pm\ell,p} \triangleq \mathrm{HE}^{\mathrm{e}}_{(\ell+1),p} \pm j\mathrm{HE}^{\mathrm{o}}_{(\ell+1),p} = \mathrm{HE}_{\pm(\ell+1),p} \qquad \text{with} \quad \ell \geq 0, \tag{3a}$$

$$\mathrm{OAM}^{\mp}_{\pm\ell,p} \triangleq \mathrm{EH}^{\mathrm{e}}_{(\ell-1),p} \pm j\mathrm{EH}^{\mathrm{o}}_{(\ell-1),p} = \mathrm{EH}_{\pm(\ell-1),p} \qquad \text{with} \quad \ell \geq 2, \tag{3b}$$

where superscripts represent left-handed ("+") or right-handed ("-") circular polarization, and p indicates the number of intensity rings of the mode. According to Eq. (3), OAM modes are defined as the helical phase-fronts representation of the HE and EH modes, whose expressions in the circular polarization basis is given in Eq. (2). Because of this definition, in the weakly guiding case, OAM modes have essentially a single OAM beam of order ℓ, with the circular polarization being built from the scalar LP modes. However, in the case of high refractive index contrast between cladding and core, they have two contributing opposite circularly polarized OAM beams of orders ℓ and $\ell \pm 2$. We continue to use the terms dominant and secondary components, with the order ℓ mode dominant. The presence of a secondary component, which has been described as the manifestation of a spin-orbit coupling effect [14, 15], makes the propagating OAM modes not pure [16, 17]. Note also that, as they are defined in Eq. (3), $\mathrm{OAM}^{\pm}_{\pm\ell,p}$ and $\mathrm{OAM}^{\mp}_{\pm\ell,p}$ constitute two 2-mode groups of degenerate modes: $\mathrm{OAM}^{+}_{+\ell,p}$ and $\mathrm{OAM}^{-}_{-\ell,p}$, and $\mathrm{OAM}^{-}_{+\ell,p}$ and $\mathrm{OAM}^{+}_{-\ell,p}$, respectively.

TE and TM are not included in the definition of Eq. (3); however, as long as they propagate, their interactions with the OAM modes must be carefully analyzed. To this end, it is convenient to express their fields in circular components as previously done for the hybrid modes. In general, the cylindrical field components of $\mathrm{TE}_{0,p}$ and $\mathrm{TM}_{0,p}$ can be expressed as [11]

$$\mathbf{E}^{\left\{\substack{\mathrm{TE}\\\mathrm{TM}}\right.}(r,\varphi) = \begin{cases} 0 \\ d(r) \end{cases} \hat{\mathbf{r}} + \begin{cases} -d(r) \\ 0 \end{cases} \hat{\boldsymbol{\varphi}} + j \begin{cases} 0 \\ e(r) \end{cases} \hat{\mathbf{z}}, \tag{4}$$

where d and e are real valued functions that do not depend on the azimuthal coordinate φ. Once expressed in circular polarizations, TE and TM fields have a form similar to Eq. (2):

$$\mathbf{E}^{\left\{\substack{\mathrm{TE}\\\mathrm{TM}}\right.}(r,\varphi) = \frac{1}{\sqrt{2}} \begin{cases} jd(r) \\ d(r) \end{cases} \exp(-j\varphi)\,\hat{\mathbf{L}} + \frac{1}{\sqrt{2}} \begin{cases} -jd(r) \\ d(r) \end{cases} \exp(j\varphi)\,\hat{\mathbf{R}} + j \begin{cases} 0 \\ e(r) \end{cases} \hat{\mathbf{z}}, \tag{5}$$

where the LCP and RCP components have the same intensity but opposite-handed helical phase-fronts of order 1. Hence, TE and TM modes do not have a dominant component and both are made of two OAM beams with topological charges +1 and −1. In weakly-guiding fibers, the $\mathrm{TE}_{0,p}$ and $\mathrm{TM}_{0,p}$ are quasi-degenerate, hence they can be linearly combined to form two modes made of a single OAM beam of order ±1. Nevertheless, since they are not exactly degenerate,

Optics EXPRESS

the resulting OAM modes are unstable; for this reason, they are not used in OAM-multiplexed transmissions and are considered "parasitic" modes [18].

The OAM and the type (dominant or secondary) of each circularly polarized field component are summarized in Table 1 for the OAM, TE and TM modes set, where $\ell \geq 0$ for the $\mathrm{OAM}^{\pm}_{\pm\ell,p}$ modes and $\ell \geq 2$ for the $\mathrm{OAM}^{\mp}_{\pm\ell,p}$ ones, in agreement with the OAM definitions in Eq. (3).

Table 1. Components of OAM, TE and TM modes. Shaded cells indicate the secondary component (or polarization). For example, $\mathrm{OAM}^{-}_{-\ell,p}$ has dominant RCP component of order $-\ell$, secondary LCP component of order $-(\ell+2)$, and longitudinal component of order $-(\ell+1)$.

Mode	Component			
	$\hat{\mathbf{L}}$	$\hat{\mathbf{R}}$	$\hat{\mathbf{z}}$	
$\mathrm{OAM}^{+}_{+\ell,p}$	ℓ	$\ell+2$	$\ell+1$	$\ell \geq 0$
$\mathrm{OAM}^{-}_{-\ell,p}$	$-(\ell+2)$	$-\ell$	$-(\ell+1)$	
$\mathrm{OAM}^{-}_{+\ell,p}$	$\ell-2$	ℓ	$\ell-1$	$\ell \geq 2$
$\mathrm{OAM}^{+}_{-\ell,p}$	$-\ell$	$-(\ell-2)$	$-(\ell-1)$	
$\mathrm{TE}_{0,p}$	1	-1	—	
$\mathrm{TM}_{0,p}$	1	-1	0	

3. Coupling relations for OAM modes

In an ideal fiber, isotropic with circular symmetry, the set of the N propagating modes is orthogonal and the propagation is described only by their propagation constants $\beta_1, \ldots, \beta_N$. In realistic fibers, several kinds of perturbation (e.g., stress birefringence, core ellipticity, twisting and bending) break the orthogonality, inducing modes to couple. In this case, mode propagation is described by coupled-mode theory as [19]

$$\frac{\mathrm{d}\mathbf{c}}{\mathrm{d}z} = -j\left(\mathbf{D} + \mathbf{K}(z)\right)\mathbf{c}(z), \tag{6}$$

where $\mathbf{c}$ is the N-dimensional vector whose elements are the complex amplitudes of the modes, $\mathbf{D} = \mathrm{diag}(\beta_1, \ldots, \beta_N)$ is the diagonal matrix of the mode propagation constants and $\mathbf{K}(z)$ is the $N \times N$ coupling matrix that accounts for the local effects of perturbations. The coupling matrix depends on the perturbation $\boldsymbol{\delta\epsilon}(r, \varphi)$ of the dielectric tensor $\boldsymbol{\epsilon}(r, \varphi)$, and for small perturbations its coefficients are given by the overlap integral [19]

$$K_{\mu\nu} = \frac{\omega}{4P}\int_0^{\infty}\int_0^{2\pi} r\,\mathbf{E}^*_{\mu}\boldsymbol{\delta\epsilon}\,\mathbf{E}_{\nu}\,\mathrm{d}\varphi\mathrm{d}r, \tag{7}$$

where ω is the angular frequency, $\mathbf{E}_{\mu}(r, \varphi)$ and $\mathbf{E}_{\nu}(r, \varphi)$ are the electric fields of modes μ and ν, and P is a normalization coefficient defined by the orthogonality condition

$$\int_0^{\infty}\int_0^{2\pi} r\left(\mathbf{E}_{\nu}\times\mathbf{H}^*_{\mu} + \mathbf{E}^*_{\mu}\times\mathbf{H}_{\nu}\right)\cdot\hat{\mathbf{z}}\,\mathrm{d}\varphi\mathrm{d}r = \delta_{\mu\nu}P, \tag{8}$$

with $\mathbf{H}_{\mu}$ and $\mathbf{H}_{\nu}$ being the magnetic fields of the two modes and $\delta_{\mu\nu}$ being the Kronecker delta.

The analytical solution of the overlap integral is difficult because of the nontrivial dependency on the radial coordinate of the fields. However, some necessary conditions for mode field components to couple can be drawn by simple considerations of the tensorial structure of $\boldsymbol{\delta\epsilon}$ and

Optics EXPRESS

the subsequent integration over φ [8, 20]. Coupling between the i-th and j-th field components of modes μ and ν can occur only if the (i, j) element of $\boldsymbol{\delta\epsilon}$ is not zero, i.e., $\delta\epsilon_{ij}(r, \varphi) \neq 0$. In many cases of practical interest $\delta\epsilon_{ij}(r, \varphi)$ can be expressed as the product of two factors, one depending on the radial coordinate and the other on the azimuthal one [20]. Since the perturbation on the fiber must be single-valued, the azimuthal function is periodic in 2π and consists of terms like $\exp(jk\varphi)$, where $k = 0, \pm 1, \ldots$ is the integer defining the azimuthal order of the perturbation. On the other hand, for Eqs. (2) and (5), the i-th component of the generic mode μ, whether OAM, TE or TM, is proportional to a factor $\exp(jq_{\mu,i}\varphi)$, where $q_{\mu,i}$ are reported in Table 1. As a consequence, the integrand in Eq. (7) includes terms that are products of exponentials with imaginary arguments, and the integration with respect to φ can be non-zero only if

$$q_{\mu,i} - q_{\nu,j} = k, \tag{9}$$

for at least a pair of field components i, j.

From a physical point of view, Eq. (9) represents the case in which the helical distribution of the perturbation matches the difference between the OAM carried by the two considered components, thus allowing for possible interaction between them. Note that the secondary and longitudinal components almost vanish in the weak-guidance limit, therefore they weakly interact with the other components and the resulting coupling is negligible. We finally remark that the condition of Eq. (9) is a necessary but not sufficient requirement for coupling to occur: $K_{\mu\nu}$ may still be zero because of the integration over the radial coordinate, which is, however, not easy to evaluate in general.

While these arguments apply to any kind of perturbations, in the following we restrict our analysis to the intrinsic ones, i.e., those potentially induced during fiber production and not necessarily caused by the external environment. These intrinsic perturbations are stress birefringence and core ellipticity. We consider the case in which the perturbations are aligned to the reference frame in this section. While this is a special condition that affects the coupling coefficients, it has no influence on the coupling conditions we discuss. The general case will be analyzed in Sec. 4.

3.1. Stress birefringence

In a fiber affected by stress birefringence, the material becomes slightly anisotropic and the tensor of the dielectric perturbation inside the h-th ring, expressed in circular components, is [20]

$$\boldsymbol{\delta\epsilon}_h(r, \varphi) = \epsilon_0 n_h \Delta n_h \begin{pmatrix} 0 & 1 & 0 \\ 1 & 0 & 0 \\ 0 & 0 & 0 \end{pmatrix}, \qquad r_{h-1} \leq r \leq r_h, \qquad h = 1, 2, \ldots \tag{10}$$

where ϵ_0 is the vacuum permittivity, and n_h, Δn_h and r_h are the refractive index, the *birefringence* and the outer radius of the h-th ring ($r_0 = 0$), respectively. By inspection of the perturbation tensor, coupling may occur only between cross-polarized transverse components ($\hat{\mathbf{L}} \leftrightarrow \hat{\mathbf{R}}$) since the particular structure of the tensor prevents all the other possible interactions. Moreover, stress birefringence does not exhibit an azimuthal dependency, that is, $k = 0$ and the corresponding coupling condition restricts coupling to components carrying the same OAM. Thanks to the previous considerations, Eq. (9) reduces to

$$q_{\mu,i} = q_{\nu,j}, \tag{11}$$

where i and j are cross-polarized transverse components. As a consequence, there cannot be coupling between TE and TM modes since opposite circular polarizations carry OAM with

Optics EXPRESS

different topological charges for such modes. The selection rules for birefringence-induced coupling are obtained from Eq. (11) and are reported in Table 2 for OAM and parasitic modes. This table covers the strongly guiding case; secondary components disappear in the weakly guiding limit.

Table 2. Selection rules for the birefringence-induced coupling; integers n and m are either ≥ 0 or ≥ 2 as specified in Eq. (3). Lack of coupling is due to polarization orthogonality (—) or Eq. (11) not being met (--). Shaded circular polarizations indicate secondary components. The lower triangular part of the table is obtained from the upper one simply by swapping n with m. TE and TM modes never couple to one another so these are not included.

$\mathrm{OAM}^{+}_{+m,p}$		$\mathrm{OAM}^{-}_{-m,p}$		$\mathrm{OAM}^{-}_{+m,p}$		$\mathrm{OAM}^{+}_{-m,p}$		Modes and Components
$\hat{\mathbf{R}}$	$\hat{\mathbf{L}}$	$\hat{\mathbf{R}}$	$\hat{\mathbf{L}}$	$\hat{\mathbf{R}}$	$\hat{\mathbf{L}}$	$\hat{\mathbf{R}}$	$\hat{\mathbf{L}}$	
—	$m=1$	—	--	—	$m=3$	—	--	$\hat{\mathbf{R}}$ TE/TM
--	—	$m=1$	—	--	—	$m=3$	—	$\hat{\mathbf{L}}$
—	$m-n=2$	—	--	—	$m-n=4$	—	--	$\hat{\mathbf{R}}$ $\mathrm{OAM}^{+}_{+n,q}$
$n-m=2$	—	$n=m=0$	—	$n=m$	—	$n+m=2$	—	$\hat{\mathbf{L}}$
		—	$n-m=2$	—	$m+n=2$	—	$n=m$	$\hat{\mathbf{R}}$ $\mathrm{OAM}^{-}_{-n,q}$
		$m-n=2$	—	--	—	$m-n=4$	—	$\hat{\mathbf{L}}$
				—	$m-n=2$	—	--	$\hat{\mathbf{R}}$ $\mathrm{OAM}^{-}_{+n,q}$
				$n-m=2$	—	$n+m=4$	—	$\hat{\mathbf{L}}$
						—	$n-m=2$	$\hat{\mathbf{R}}$ $\mathrm{OAM}^{+}_{-n,q}$
						$m-n=2$	—	$\hat{\mathbf{L}}$

3.2. *Core ellipticity*

Core ellipticity consists of a slight deformation of the ideal circular shape of the fiber cross-section. This deformation yields the scalar dielectric perturbation [20]

$$\boldsymbol{\delta\epsilon}(r,\varphi) = \epsilon_0 \cos 2\varphi \sum_{h=1}^{R-1} \gamma_h (n_h^2 - n_{h+1}^2)\, \delta(r - r_h), \tag{12}$$

where $\delta(\cdot)$ is the Dirac function, subscript h selects one of the R rings of the fiber and γ_h is *elliptical deformation* in terms of maximum radius variation. As in the stress birefringence case, the particular structure of the perturbation determines the possible interactions among the components, but this time, since the perturbation is scalar, core ellipticity allows coupling only between the same components ($\hat{\mathbf{R}} \leftrightarrow \hat{\mathbf{R}}$, $\hat{\mathbf{L}} \leftrightarrow \hat{\mathbf{L}}$ or $\hat{\mathbf{z}} \leftrightarrow \hat{\mathbf{z}}$). Moreover, the perturbation presents a dependency on φ through a sinusoidal function of azimuthal order $k = \pm 2$. Putting together these observations, the coupling condition in Eq. (9) becomes

$$q_{\mu,i} - q_{\nu,i} = 2 \quad \text{or} \quad q_{\nu,i} - q_{\mu,i} = 2 \tag{13}$$

where i selects the same component in each mode. A closer examination of Table 1 reveals that the condition is actually the same for every selected kind of component in each couple of modes. Therefore, the selection rules depend on the chosen modes but not on the choice of the specific component. Selection rules for ellipticity-induced coupling are summarized in Table 3. Again, results are for the strongly guiding case; modes with opposite dominant components should not be considered in the weak-guidance limit. Indeed, in that case, the eventual coupling comes from interactions involving secondary or longitudinal components, which are nevertheless negligible.

Optics EXPRESS

Table 3. Selection rules for the ellipticity-induced coupling among OAM, TE and TM modes, where they are reported once for each mode combination. Integers n and m are either ≥ 0 or ≥ 2, as specified in Eq. (3). Symbol -- means that the corresponding condition in Eq. (13) is never verified by the specific mode orders. Shaded circular polarizations indicate secondary components. The lower triangular part of the table is obtained from the upper one simply by swapping n with m.

TE/TM		$\mathrm{OAM}^{+}_{+m,p}$		$\mathrm{OAM}^{-}_{-m,p}$		$\mathrm{OAM}^{-}_{+m,p}$		$\mathrm{OAM}^{+}_{-m,p}$		Modes and Components	
$\hat{\mathbf{R}}$	$\hat{\mathbf{L}}$	$\hat{\mathbf{R}}$	$\hat{\mathbf{L}}$	$\hat{\mathbf{R}}$	$\hat{\mathbf{L}}$	$\hat{\mathbf{R}}$	$\hat{\mathbf{L}}$	$\hat{\mathbf{R}}$	$\hat{\mathbf{L}}$	TE/TM	
--		$m = 1$		$m = 1$		$m = 3$		$m = 3$		$\hat{\mathbf{R}}$	$\hat{\mathbf{L}}$
		$\lvert m - n\rvert = 2$		$m = n = 0$		$m - n = 4$ $m = n$		$m + n = 2$		$\mathrm{OAM}^{+}_{+n,q}$ $\hat{\mathbf{R}}$	$\hat{\mathbf{L}}$
				$\lvert m - n\rvert = 2$		$m + n = 2$		$m = n$ $m - n = 4$		$\mathrm{OAM}^{-}_{-n,q}$ $\hat{\mathbf{R}}$	$\hat{\mathbf{L}}$
						$\lvert m - n\rvert = 2$		$m = n = 0$ $m = n = 2$		$\mathrm{OAM}^{-}_{+n,q}$ $\hat{\mathbf{R}}$	$\hat{\mathbf{L}}$
								$\lvert m - n\rvert = 2$		$\mathrm{OAM}^{+}_{-n,q}$ $\hat{\mathbf{R}}$	$\hat{\mathbf{L}}$

4. Numerical analysis of power coupling

To verify the accuracy of the coupling relations and to study the propagation of OAM modes in stress birefringence- and core ellipticity-affected fibers, we consider a *hollow ring-core fiber* for OAM transmission [9] and numerically assess its propagation properties in terms of power coupling. In the following, we first describe the model of propagation, then we evaluate both fiber propagation constants and coupling coefficients, and finally we assess power coupling from Monte Carlo simulations of the fiber.

4.1. Numerical model of propagation

The complex amplitudes of the modes at a given point z along the fiber are given by

$$\mathbf{c}(z) = \mathbf{U}(z)\,\mathbf{c}(z_0), \tag{14}$$

where the propagation operator $\mathbf{U}$ is an $\mathrm{N}\times\mathrm{N}$ complex matrix that includes the cumulative effects of all the interactions occurred among modes up to z. In these settings, mode coupling can be fully characterized by the study of $\mathbf{U}$, whose evolution is given by the differential equation [21]

$$\frac{\mathrm{d}\mathbf{U}}{\mathrm{d}z} = -j\left(\mathbf{D} + \mathbf{K}(z)\right)\mathbf{U}(z) = -j\,\mathbf{B}(z)\,\mathbf{U}(z), \tag{15}$$

obtained by combining Eqs. (6) and (14), and defining $\mathbf{B}(z) = \mathbf{D} + \mathbf{K}(z)$. Note that, although the matrix $\mathbf{K}(z)$ represents the *local* coupling between modes, the overall *accumulated* coupling depends also on matrix $\mathbf{D}$. As a rule of thumb, the larger the difference between the propagation constants, the lower the coupling between the modes. To describe concisely the properties of the fiber, we introduce two parameters: the fiber modal birefringence $\Delta\beta$, that characterizes the maximum separation among modes; and the coupling strength $\Delta\kappa$, that characterizes the maximum relative strength of the perturbations. Accordingly, we define these parameters as:

$$\Delta\beta = \max\beta_i - \min\beta_i \quad \text{and} \quad \Delta\kappa = \max\kappa_i - \min\kappa_i, \tag{16}$$

Optics EXPRESS

where $\kappa_i \in \mathrm{eig}(\mathbf{K})$. Modal birefringence and coupling strength can be expressed also in terms of beat lengths, where the modal and coupling beat lengths are respectively given by $L_\beta = 2\pi/\Delta\beta$ and $L_\kappa = 2\pi/\Delta\kappa$.

Since the perturbations evolve randomly along the fiber, the corresponding coupling matrices should be evaluated for an arbitrary strength and orientation of perturbation. However, the coupling matrix $\mathbf{K}$ for the single perturbation ξ can be written as $\alpha\mathbf{M}(\theta)\,\mathbf{K}_{\xi_0}\,\mathbf{M}^{\mathrm{T}}(\theta)$, where $\mathbf{K}_{\xi_0}$ is the coupling matrix for the reference perturbation ξ_0, which is of the same kind of ξ but aligned to the reference frame and normalized in strength; α is the coefficient that accounts for the relative variation of the perturbation strength with respect to ξ_0; θ is the angle at which the perturbation is oriented with respect to the reference frame; and $\mathbf{M}$ is a proper rotation operator [8, 20]. As stated before, a rotation of the perturbation does not change the coupling condition of Eq. (9); therefore the operator $\mathbf{M}$ is a block diagonal matrix where each block corresponds to a group of degenerate modes. With respect to the hybrid modes of order υ, these blocks are given by

$$\mathbf{T}(\upsilon\theta) = \frac{1}{\sqrt{2}}\begin{pmatrix} \exp\left(-j\upsilon\theta\right) & \exp\left(j\upsilon\theta\right) \\ j\exp\left(-j\upsilon\theta\right) & -j\exp\left(j\upsilon\theta\right) \end{pmatrix}. \tag{17}$$

As a consequence, according to Eq. (3), the diagonal blocks are $\mathbf{T}^{\pm}(\ell\theta) = \mathbf{T}((\ell+1)\,\theta)$ for the $\mathrm{OAM}^{\pm}_{\pm\ell}$ mode groups; whereas they are $\mathbf{T}^{\mp}(\ell\theta) = \mathbf{T}((\ell-1)\,\theta)$ for the $\mathrm{OAM}^{\mp}_{\pm\ell}$ ones. For TE and TM modes, $\mathbf{T} = 1$ because these modes are not degenerate, they have cylindrical symmetry and rotation has no effects on them.

When there are more kinds of perturbation, the total coupling matrix is the superposition of each single contribution applied with its own angle θ_ξ and magnitude α_ξ, which generally vary along the fiber. Therefore, the final expression of matrix $\mathbf{B}$ is

$$\mathbf{B}(z) = \mathbf{D} + \sum_{\xi} \alpha_\xi(z)\mathbf{M}\big(\theta_\xi(z)\big)\mathbf{K}_{\xi_0}\mathbf{M}^{\mathrm{T}}\big(\theta_\xi(z)\big), \tag{18}$$

where the summation is extended to the different kinds of perturbation ξ affecting the fiber.

As stated above, we limit the analysis to stress birefringence and core ellipticity. These two perturbations arise mainly from the manufacturing process, so it is reasonable to assume that birefringence axes are aligned to the ones of the elliptical core [22, 23]. Following the guidelines of the so-called *fixed-modulus model*, introduced to describe polarization mode dispersion in single mode fibers [24], we assume the coefficients $\alpha_{\mathrm{B}}(z)$ and $\alpha_{\mathrm{E}}(z)$ to be constant for birefringence and ellipticity, respectively. As a consequence, the overall coupling strength $\Delta\kappa$ is also constant along the fiber, and we can write

$$\mathbf{B}(z) = \mathbf{D} + \mathbf{M}(\theta(z))\left[\alpha_{\mathrm{B}}\mathbf{K}_{\mathrm{B}_0} + \alpha_{\mathrm{E}}\mathbf{K}_{\mathrm{E}_0}\right]\mathbf{M}^{\mathrm{T}}(\theta(z)), \tag{19}$$

where $\theta(z)$ is the common orientation of the perturbations, and $\mathbf{K}_{\mathrm{B}_0}$ and $\mathbf{K}_{\mathrm{E}_0}$ are the coupling matrices of the corresponding reference perturbations reported in Eqs. (10) and (12). According to this model, the values of birefringence Δn_h and of elliptical deformation γ_h should be chosen to have reference perturbations of normalized strength; whereas the coefficients α_{B} and α_{E} determine the ratio between the two perturbations and the overall coupling strength $\Delta\kappa$. Regarding the orientation of the perturbations, again following the fixed-modulus model, we describe $\theta(z)$ as a Wiener process [24, 25]:

$$\frac{\mathrm{d}\theta}{\mathrm{d}z} = -\sigma\eta(z), \tag{20}$$

where η is a Gaussian white noise of zero mean and unitary variance, and σ parametrizes the correlation of the process. According to [24], we define the correlation length $L_{\mathrm{F}} = 1/(2\sigma^2)$.

Optics EXPRESS

The above model has been numerically implemented by using the wave-plate model, which consists in discretizing the propagation through a cascade of D fiber sections, called plates [25–28]. The operator $\mathbf{U}_k$, that describes propagation from the fiber input to the k-th plate is given by $\mathbf{U}_k = \mathbf{W}_k\mathbf{U}_{k-1}$, where $\mathbf{W}_k$ accounts for the propagation through the k-th plate. The length L_s of each plate is chosen to be so short that the coupling matrix $\mathbf{K}(z)$ can be assumed constant within the plates. Therefore, $\mathbf{W}_k = \exp(-j\mathbf{B}_k\mathrm{L}_s)$ where

$$\mathbf{B}_k = \mathbf{D} + \mathbf{M}(\theta_k)\left[\alpha_{\mathrm{B}}\mathbf{K}_{\mathrm{B}_0} + \alpha_{\mathrm{E}}\mathbf{K}_{\mathrm{E}_0}\right]\mathbf{M}^{\mathrm{T}}(\theta_k), \tag{21}$$

and θ_k is the constant orientation of the perturbations inside the k-th plate. According to Eq. (20), $\theta_k - \theta_{k-1} = -\mathrm{L}_s\sigma\eta_k$, where η_k are i.i.d. Gaussian variables of zero mean and unitary variance.

4.2. Application to hollow ring-core fiber

We analyzed a hollow ring-core fiber, whose index profile is defined in Fig. 1. Modal properties have been numerically calculated with ComSol at 1550 nm; the fiber supports 26 information bearing OAM modes and the two parasitic $\mathrm{TE}_{0,1}$ and $\mathrm{TM}_{0,1}$ modes. The corresponding effective refractive indexes are represented in Fig. 2, where degenerate OAM modes are grouped in the 2-mode groups $\mathrm{OAM}^{\pm}_{\pm\ell,p}$ and $\mathrm{OAM}^{\mp}_{\pm\ell,p}$; the fiber modal beat-length is $L_\beta = 161\ \mu$m. Note that OAM 7 modes are present only within the $\mathrm{OAM}^{\pm}_{\pm 7}$ group, which is close to the cut-off and far from the other groups in terms of propagation constants. For these reasons, we expect these modes to be less affected by coupling than the others.

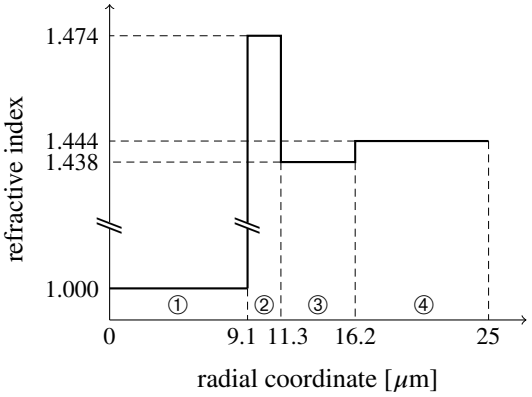

	Outer Radii [μm]	Refractive Indices
① Air-hole	9.1	1.000
② Ring-core	11.3	1.474
③ Trench	16.2	1.438
④ Cladding	25	1.444

Fig. 1. Hollow ring-core fiber index profile with $h = 4$ rings.

The mode coupling coefficients have been calculated by computing numerically the overlap integrals of Eq. (7) for the reference perturbations in Eqs. (10) and (12). In particular, for stress birefringence, we assume that the birefringence Δn is equal for all the rings, except for the inner air core, for which of course $\Delta n = 0$. Similarly, regarding core ellipticity, we assume that the elliptical deformation γ is the same for all rings. Figure 3 shows the coupling coefficients for both stress birefringence and core ellipticity, each normalized to their corresponding absolute maximum. The figure should be read in relation to the selection rules of Tables 2 and 3. In particular, to show the agreement with the selection rules, different marks have been used to highlight the strongest modal interaction that origins the coupling. Marks "□" describe coupling between dominant components, which is generally the strongest; marks "◇" describe coupling between the secondary ones, which is the weakest; and marks "○" describe dominant-secondary mixed coupling. Coupling coefficients marked with "○" or "◇" become negligible in weakly

Optics EXPRESS

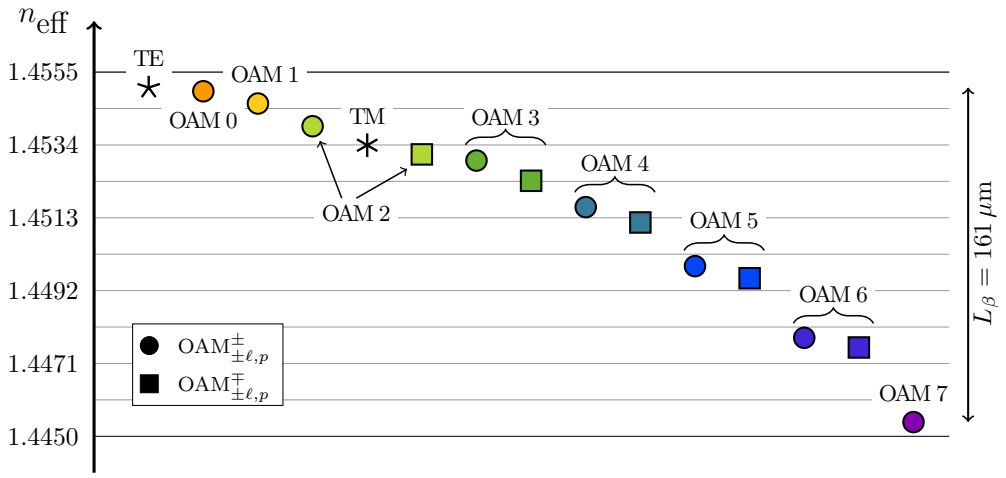

Fig. 2. Effective refractive indexes for the groups of degenerate modes. Symbols ● and ■ refer to $\text{OAM}^{\pm}_{\pm\ell,p}$ and $\text{OAM}^{\mp}_{\pm\ell,p}$ respectively, while TE and TM modes are depicted with ✶ and ∗ symbols. Colors indicate different OAM orders.

guiding fibers but are non-negligible in this strongly guiding fiber. Note that marks in Fig. 3 do not describe exhaustively all the modal interactions occurring between the components of two modes, but just denote the strongest possible one; whereas the intensity of the coefficients are given by the contribution of all of them. Furthermore, given the fields expressions of Eqs. (2) and (5) and the perturbations in Eqs. (10) and (12), the coupling coefficients are all reals except for those involving TE modes, which are imaginary. This is denoted in Fig. 3 by a black dot in the corresponding cells.

As theoretically predicted, stress birefringence and core ellipticity induce the same coupling pattern among modes, but with different intensities. Indeed, most of the dominant-dominant interactions ("□") for the birefringence correspond to dominant-secondary interactions ("○") for the ellipticity and vice versa. Moreover, while the two perturbations induce coupling of the same sign on the fundamental modes, which is in agreement with [23], the coupling coefficients of higher order modes and close to the main diagonal appear of opposite sign. As a consequence, since the coupling coefficients along the main diagonal are the ones that mostly affect coupling, the contributions of birefringence and ellipticity tend to partially compensate one another. The compensation depends on the relative strength of the perturbations; however, when the two contributions to the fundamental modes are comparable, as pointed out in [23], the compensation is in general small. This is exactly the case represented in Fig. 3, where the ellipticity-induced coupling close to the main diagonal is weak because due to dominant-secondary interactions and cannot compensate the birefringence-induced one.

Finally, the coupling coefficients for the parasitic modes are not negligible, with TE_{01} and TM_{01} coupling significantly to $\text{OAM}^{\pm}_{\pm1}$ and $\text{OAM}^{\mp}_{\pm3}$ groups. Therefore, we expect the coupling involving parasitic modes to be significant during propagation.

4.3. Numerical propagation

The propagation along the fiber has been numerically simulated for coupling strength values in the range of $\text{L}_\beta/\text{L}_\kappa \in [10^{-4}, 10^{-1}]$ and for two different fiber correlation lengths, $L_\text{F} \in \{1\,\text{m}, 10\,\text{m}\}$ [29]. For each value of coupling strength, different combinations of birefringence and ellipticity coefficients α_B and α_E have been considered. However, we report just the cases

Optics EXPRESS

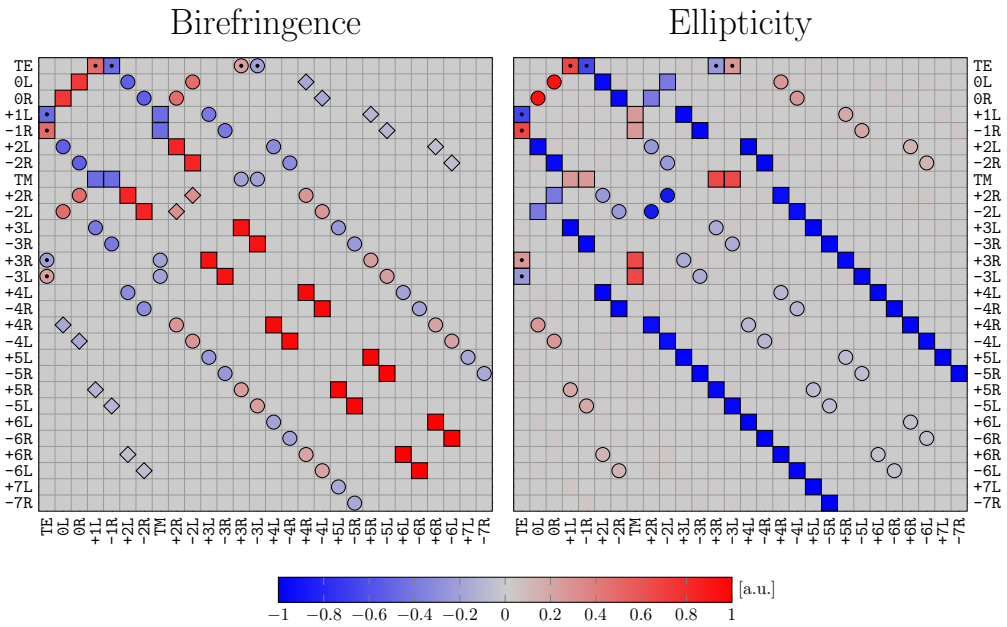

Fig. 3. Coupling coefficients computed numerically from the overlap integral in Eq. (7), for stress birefringence and core ellipticity, each normalized to their corresponding absolute maximum. Marks indicate the strongest interaction that contribute to the coefficient: "□" represents interactions between dominant components, "○" refers to dominant-secondary mixed interactions, and "◇" indicate interactions between secondary components. All the elements are real except those marked with a black dot, which are purely imaginary.

in which either only birefringence ($\alpha_B = 1$ and $\alpha_E = 0$) or only ellipticity ($\alpha_B = 0$ and $\alpha_E = 1$) affects the fiber, since the intermediate cases are trivial combinations of the two and do not provide further insight. The fibers were modeled with 100 000 plates of length $L_s = L_F/100$, so as to have the perturbation orientation almost constant within plates. An ensemble of 15 000 random realizations of the fiber has been collected for the statistical analysis.

We have used averaging over the statistical ensemble to characterize the power coupling between the degenerate mode groups $\mathrm{OAM}^{\pm}_{\pm\ell,p}$ and $\mathrm{OAM}^{\mp}_{\pm\ell,p}$, which has a direct impact on the complexity of multi-input multi-output (MIMO) receivers [5], while we chose not to treat here the coupling within each degenerate OAM group. We characterize power coupling by showing: 1) the average power as a function of distance in each group of degenerate modes; and 2) the cross-talk at 1 km, defined as the average normalized power transfered from one input group to all others after 1 km.

The normalized average power on each group when the power is launched on that group is plotted in Fig. 4 as a function of distance for both birefringence and ellipticity and for $L_\beta/L_\kappa = 2\times10^{-4}$, 2×10^{-3}, 2×10^{-2}, which represent weak, medium and strong perturbation regimes, respectively. Only the results for $L_F = 1$ m are shown, because those for $L_F = 10$ m are the same provided that the z-axis is proportionally rescaled. In general, all the curves in the graphs decay with distance, meaning that each launched group couples to some extend with some of the others during propagation. However, the decay is not simply exponential, as it would occur in the single-mode case [30], but has different behaviors as well as different asymptotic limits, depending on the considered groups and parameters.

Defining a decay rate coefficient to describe the average power evolution is therefore not

Optics EXPRESS

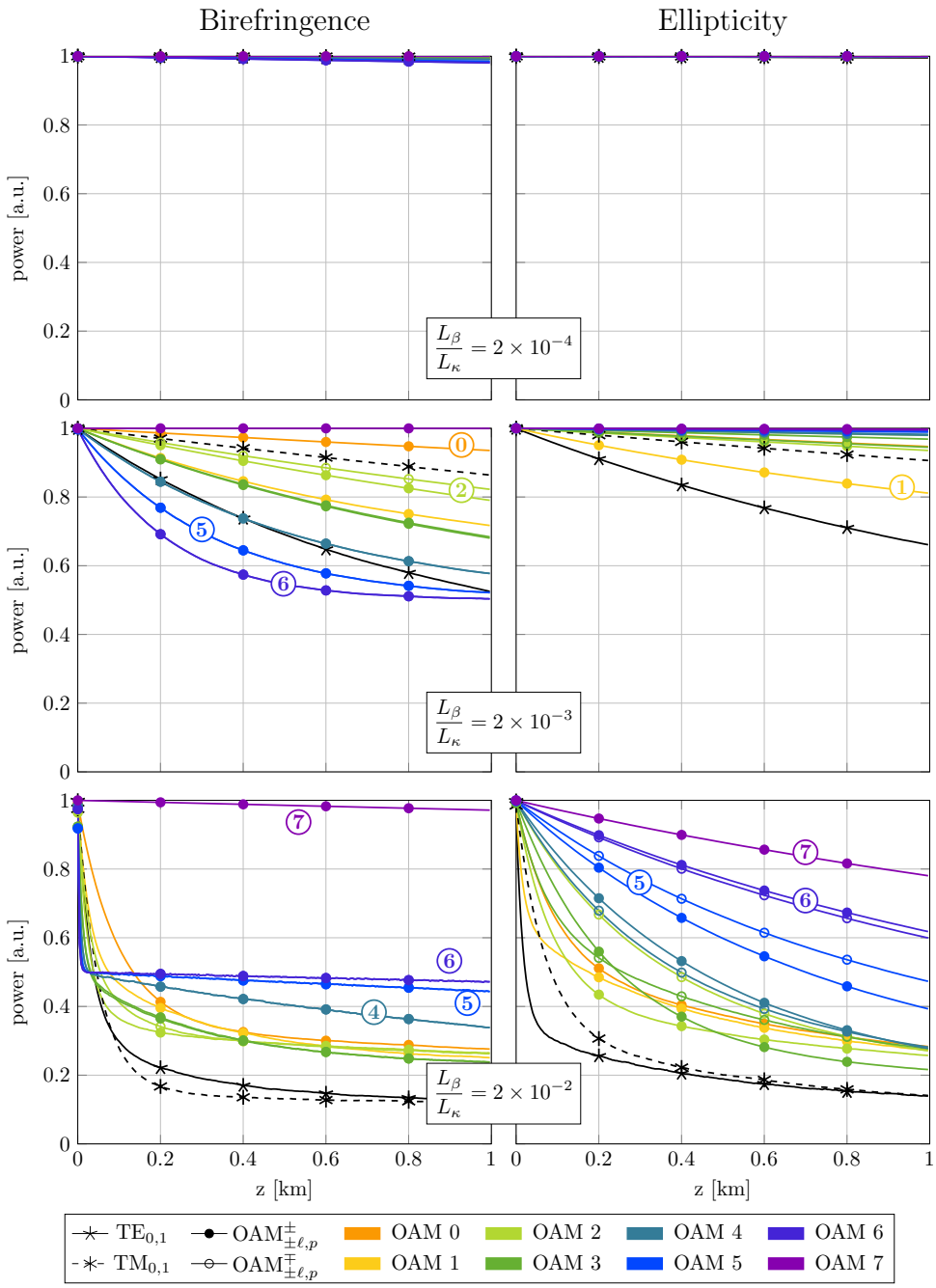

Fig. 4. Average power on each group of degenerate modes $\mathrm{OAM}^{\pm}_{\pm\ell,p}$ and $\mathrm{OAM}^{\mp}_{\pm\ell,p}$ when the power is launched on that group, represented as a function of distance for birefringence- and ellipticity-induced coupling and fiber correlation length $L_F = 1$m.

possible. For this reason, we evaluate the cross-talk at 1 km, which gives an insight on how much power spreads from one group to the others because of coupling. Figure 5 represents the

Optics EXPRESS

cross-talk generated by each group versus L_β/L_κ, for both birefringence and ellipticity and for both $L_F = 1$m and $L_F = 10$ m. Not surprisingly, cross-talk increases with the strength of the perturbations. The increase is linear for small and medium values of L_β/L_κ (weak and medium perturbation regimes), while it saturates for large ones (strong perturbation regime). However, such high values are not likely reached in real strongly-guiding fibers and represent extreme scenarios. Moreover, Fig. 5 shows that for weak and medium perturbations the crosstalk increases by about 10 dB when L_F decreases from 10 m to 1 m.

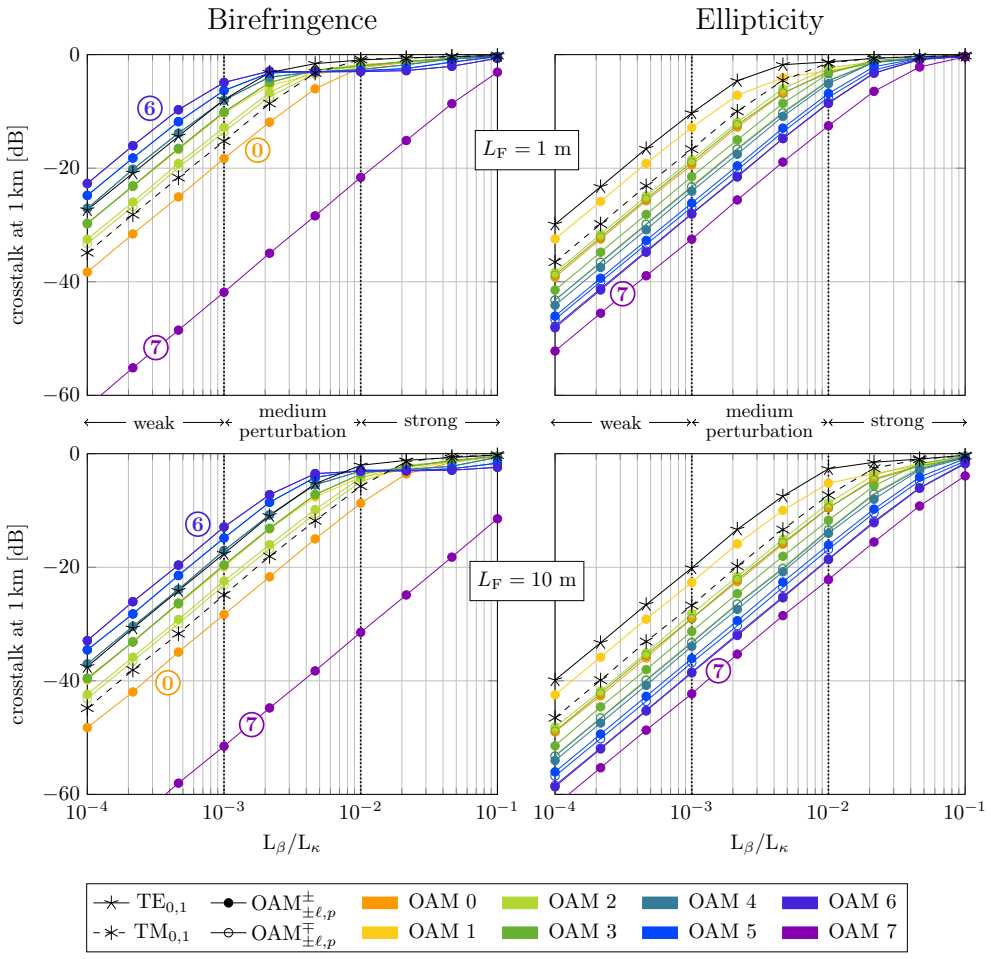

Fig. 5. Crosstalk generated by each degenerate mode group $\mathrm{OAM}^{\pm}_{\pm\ell,p}$ and $\mathrm{OAM}^{\mp}_{\pm\ell,p}$ at 1 km length, represented as a function of L_β/L_κ in case of birefringence- and ellipticity-induced coupling, with fiber correlation length of either $L_F = 1$ m or $L_F = 10$ m.

Results confirm that stress birefringence and core ellipticity have different effects on modes propagation even if they induce the very same coupling pattern among modes (Fig. 3). In particular, birefringence is the one causing the higher cross-talk because it strongly affects groups with low phase-mismatch, while this is not true for ellipticity. Indeed, the birefringence coupling matrix has the most intense coefficients closer to its diagonal, whereas the most intense coefficients for ellipticity involve modes that are more separated in terms of propagation constants. Still, both kinds of perturbation cause parasitic TE and TM modes to couple with the $\mathrm{OAM}^{\pm}_{\pm 1}$ and the

Optics EXPRESS

$\mathrm{OAM}^{\mp}_{\pm 3}$ (Fig. 3). Results show that these interactions are not negligible from the power coupling point of view, and they should be carefully considered in the design of the transmission system. Moreover, the coupling between TE and $\mathrm{OAM}^{\pm}_{\pm 1}$ explains the one experimentally observed in [18], confirming the ability of the developed model to reproduce coupling mechanisms in ring-core fibers. Finally, $\mathrm{OAM}^{\pm}_{\pm 7}$ seems the group less affected by coupling, especially in case of birefringence. We believe this represents an extreme case, due to the group being close to its cut-off condition.

4.4. Theoretical assessment of power coupling

Power coupling in multimode and multi-core fibers has been theoretically analyzed in previous literature, and average power flow is modeled as [31, 32]

$$\frac{dP_\mu(z)}{dz} = \sum_{\nu \neq \mu} h_{\mu\nu}(z) \left(P_\nu(z) - P_\mu(z)\right), \tag{22}$$

where $P_\mu(z)$ is the average power of mode μ, and $h_{\mu\nu}$ are the coefficients that describe the average power coupling between modes μ and ν along the propagation direction. These coefficients depend on matrix $\mathbf{B}(z)$ of Eq. (15) and on its statistical properties. The exact calculation of coefficients $h_{\mu\nu}$ involves stochastic calculus and can be quite involved. Nonetheless, in [32] it has been proven that, assuming a negative exponential autocorrelation function of the stationary fiber perturbation process along z, an analytical approximation of such coefficients, valid for small z, is

$$h_{\mu\nu} = \frac{2K^2_{\mu\nu} L_\mathrm{F}}{1 + \left[\Delta\beta_{\mu\nu} L_\mathrm{F}\right]^2}, \tag{23}$$

where $\Delta\beta_{\mu\nu} = |\beta_\nu - \beta_\mu|$. Since the coefficients $h_{\mu\nu}$ are z-independent, the mode powers in Eq. (22) can be easily calculated. Although this coupling result was derived for single-mode multi-core fibers with a different theoretical model of coupling, we have verified empirically that the formula provides a good approximation for the present case. This verification is given in Fig. 6, which shows the difference in dB between the crosstalk at 1 km obtained from Eq. (23) and that of the numerical crosstalk reported in Fig. 5. The coefficients $h_{\mu\nu}$ in the theoretical solution have been obtained by using the numerical values for β_μ and $K_{\nu\mu}$ (Eq. (7)) for our OAM fiber. As can be seen from Fig. 6, the theoretical crosstalk approximation is always within about 1 dB from the true numerical results. We can therefore conclude that Eqs. (22) and (23) yield reliable mode power results, provided that the actual OAM propagation and coupling coefficients are used in Eq. (23).

4.5. Assessment of SNR penalty from crosstalk

With knowledge of crosstalk at a given distance, we can determine the perturbation strength where the linear coupling starts to impact higher order modulation formats, such as quadrature phase-shift keying (QPSK) or quadrature amplitude modulation (QAM). Increasing the modulation format order induces stringent crosstalk requirements [33], particularly on OAM fibers that target limited 2×2 MIMO. These requirements have a direct impact on perturbation tolerance and provide insight on the fiber design constraints.

In [33] the signal-to-noise ratio (SNR) penalty due to crosstalk, i.e., SNR increment needed to provide the same bit error rate (BER), was quantified for a targeted BER and different modulation formats. For instance, in [33] by simulation, it has been shown that at a given BER of 10^{-3} the maximum tolerable crosstalk to have an SNR penalty of at most 1dB is about -17 dB for QPSK, -23 dB for 16-QAM, and -29 dB for 64-QAM. Those values can be straightforwardly combined with the results reported in Fig. 5 to determine which coupling strength results in a 1 dB change in SNR.

Optics EXPRESS

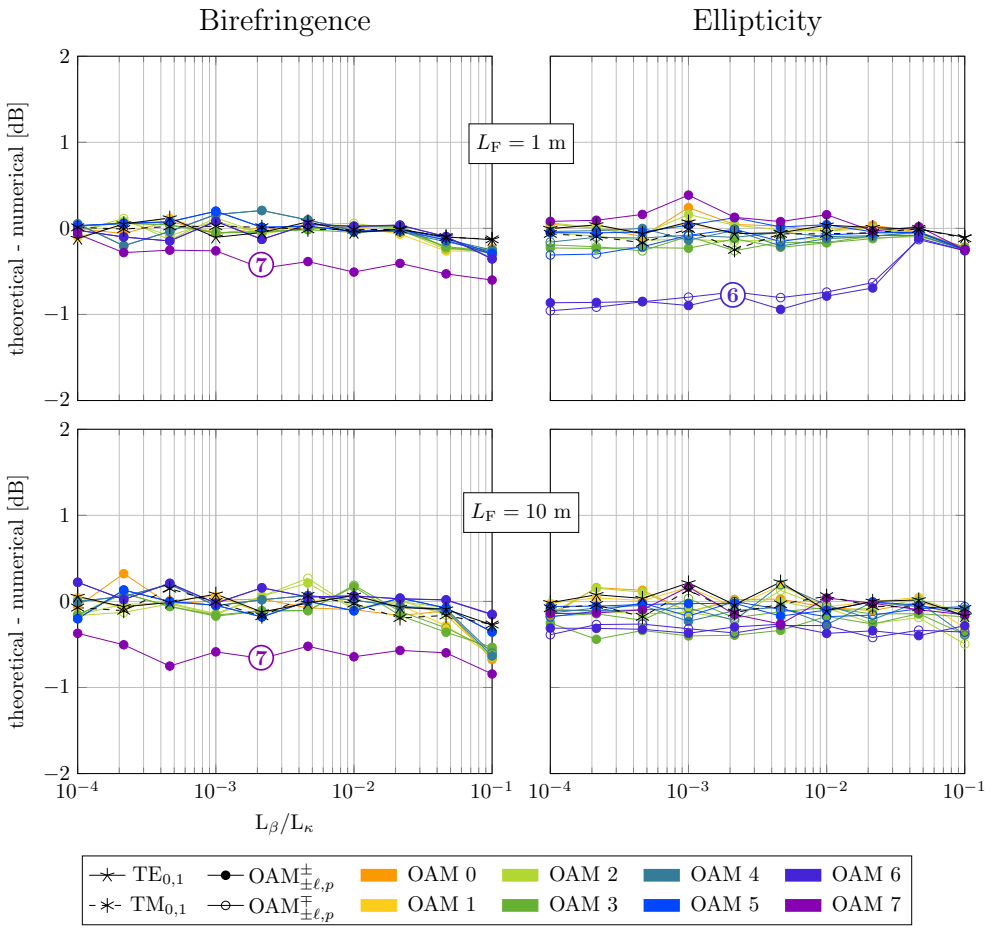

Fig. 6. Difference between the crosstalk (in dB) at 1 km evaluated from theory (Eqs. (22) and (23)) and the one obtained from numerical simulations (Fig. 5).

Assuming that the crosstalk $\mathcal{X}$ is a Gaussian noise on the desired mode, we can approximate the SNR penalty at a targeted BER for the desired modulation formats. The SNR penalty (ΔSNR) can be written in the following manner:

$$\Delta\text{SNR} = \frac{1}{\left(1 - (\text{SNR}^{\text{BER}}) \cdot \mathcal{X}\right)} \tag{24}$$

where SNR^{BER} is the SNR that provides a targeted BER. For QAM with Gray coding SNR^{BER} is written as follows [34]:

$$\text{SNR}^{\text{BER}} = \frac{M-1}{3} \cdot \left(Q^{-1}\left(\frac{1 - \sqrt{1 - \text{BER} \cdot \log_2 M}}{2\left(1 - \frac{1}{\sqrt{M}}\right)} \right) \right)^2 \tag{25}$$

where M is the modulation format order.

This approximation shows good agreement with the results in [33] up to 2 dB of SNR penalty. Beyond this limit, the Gaussian approximation becomes pessimistic. This allows us to connect

Optics EXPRESS

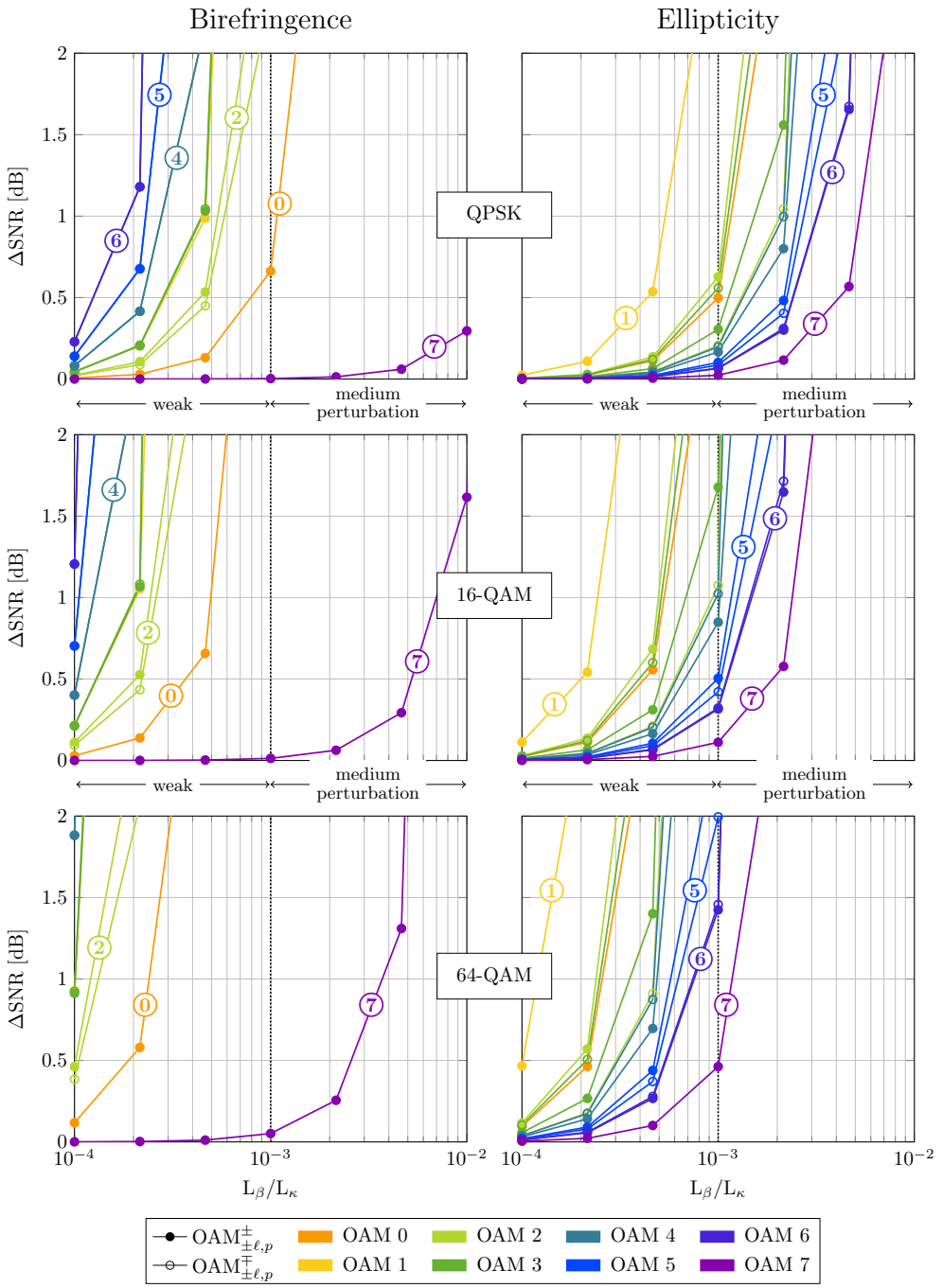

Fig. 7. SNR penalty at 1 km length for OAM transmission, represented as a function of L_β/L_κ in case of stress birefringence and core ellipticity of $L_F = 1$ m. Results are represented for different modulation formats: QPSK, 16-QAM, and 64-QAM.

the coupling strength with the SNR penalty at a given BER for the desired modulation formats. In

Optics EXPRESS

Fig. 7 we plot the SNR penalty vs. coupling strength for both stress birefringence and ellipticity for three different modulation formats (QPSK, 16-QAM, and 64-QAM) at BER of 10^{-3}. Only the $L_F = 1$ case at 1 km is reported for the sake of space. This approach can be repeated on all the perturbation correlations, link lengths, perturbation types, and modulation formats, that cause penalties below 2 dB.

In Fig. 7 we see how increasing the modulation format increases the crosstalk requirements. While these fibers are designed to avoid crosstalk, for high modulation formats, such as 64-QAM, even small modal interactions from these intrinsic fiber perturbations can significantly affect system performance. We note that already at 1 km in the case of QPSK and medium perturbation strength, the penalty due to birefringence is greater than 2 dB for most propagating modes. When increasing the modulation order to 64-QAM, a consistent portion of modes pass the 2 dB threshold even for the weakest investigated perturbation strength. These observations suggest that, when only a 2×2 MIMO on polarization is targeted and the investigated fiber is employed, the fiber reach is limited to short or ultra-short distances (i.e., data-centers).

To validate the theoretical results experimentally, including link reach for specific modulation formats, we must characterize all coupling strengths along the link. Such an effort could be feasible for short or ultra-short links where this fiber design may find its application. While outside the scope of this paper, an experimental examination would clarify the relative importance of the two contributions to coupling, birefringence and ellipticity.

5. Conclusions

We have applied classic perturbation theory for modal coupling to a very strongly guiding, air core fiber design. We identified the specific coupling mechanisms among OAM modes, highlighting the impact of modal impurities in OAM mode propagation (leading to dominant and secondary). We assess propagation properties, providing power coupling analysis in terms of accumulated crosstalk versus distance and coupling strength for stress birefringence and core ellipticity. Moreover, we observed that the theoretical crosstalk approximation of [32] is in good agreement with our numerical results. The methodology developed could be used for other strongly guiding ring core fibers.

Our results can assist in the design and development of new strongly guiding multimode fibers. First, in the context of transmission system performance simulation and prediction, accounting for both linear and nonlinear effects, a realistic and formal approach to the linear coupling in strongly guiding optical fibers is fundamental to provide accurate and meaningful results. Indeed, nonlinear effects and linear crosstalk contribute simultaneously to the propagation, and the nonlinear term cannot be simplified by the so-called generalized Manakov approach [35, 36], because of the selective coupling and the large propagation constants difference. Second, in terms of system performance analysis, an accurate knowledge of crosstalk enables, resorting to [33], a quick evaluation of penalties due to mode coupling, obtaining the maximum tolerable coupling strength at the targeted system performance at a given distance or, conversely, the maximum achievable distance given a coupling strength. Finally, our results could be used to devise experiments to better parameterize the perturbations observed in fabricated fibers.

Funding

H2020 LEIT Information and Communication Technologies (645361).

Disclosures

The authors declare that there are no conflicts of interest related to this article.

Optics EXPRESS

References

1. R. Ryf, S. Randel, A. H. Gnauck, C. Bolle, A. Sierra, S. Mumtaz, M. Esmaeelpour, E. C. Burrows, R. Essiambre, P. J. Winzer, D. W. Peckham, A. H. McCurdy, and R. Lingle, "Mode-Division Multiplexing Over 96 km of Few-Mode Fiber Using Coherent 6x6 MIMO Processing," J. Light. Technol. **30**, 521–531 (2012).
2. L. A. Rusch, M. Rad, K. Allahverdyan, I. Fazal, and E. Bernier, "Carrying Data on the Orbital Angular Momentum of Light," IEEE Commun. Mag. **56**, 219–224 (2018).
3. R. Ryf, M. A. Mestre, S. Randel, C. Schmidt, A. H. Gnauck, R. Essiambre, P. J. Winzer, R. Delbue, P. Pupalaikis, A. Sureka, Y. Sun, X. Jiang, D. W. Peckham, A. McCurdy, and R. Lingle, "Mode-Multiplexed Transmission Over a 209-km DGD-Compensated Hybrid Few-Mode Fiber Span," IEEE Photonics Technol. Lett. **24**, 1965–1968 (2012).
4. L. Wang, R. M. Nejad, A. Corsi, J. Lin, Y. Messaddeq, L. Rusch, and S. LaRochelle, "Linearly polarized vector modes: Enabling MIMO-free mode-division multiplexing," Opt. Express **25**, 11736–11749 (2017).
5. R. M. Nejad, K. Allahverdyan, P. Vaity, S. Amiralizadeh, C. Brunet, Y. Messaddeq, S. LaRochelle, and L. A. Rusch, "Mode Division Multiplexing Using Orbital Angular Momentum Modes Over 1.4-km Ring Core Fiber," J. Light. Technol. **34**, 4252–4258 (2016).
6. G. Zhu, Z. Hu, X. Wu, C. Du, W. Luo, Y. Chen, X. Cai, J. Liu, J. Zhu, and S. Yu, "Scalable mode division multiplexed transmission over a 10-km ring-core fiber using high-order orbital angular momentum modes," Opt. Express **26**, 594–604 (2018).
7. B. Ndagano, R. Brüning, M. McLaren, M. Duparré, and A. Forbes, "Fiber propagation of vector modes," Opt. Express **23**, 17330–17336 (2015).
8. L. Palmieri and A. Galtarossa, "Coupling Effects Among Degenerate Modes in Multimode Optical Fibers," IEEE Photonics J. **6**, 1–8 (2014).
9. C. Brunet, P. Vaity, Y. Messaddeq, S. LaRochelle, and L. A. Rusch, "Design, fabrication and validation of an OAM fiber supporting 36 states," Opt. Express **22**, 26117 (2014).
10. M. Lonardi, G. Guerra, L. Marcon, R. M. Nejad, M. Santagiustina, A. Galtarossa, L. A. Rusch, A. Bononi, and L. Palmieri, "Mode coupling analysis of hollow ring-core fibers for oam transmission," in 2017 European Conference on Optical Communication (ECOC), (2017), pp. 1–3.
11. A. W. Snyder and Love, J., *Optical Waveguide Theory*, Science Paperbacks (Springer, 1983).
12. L. Allen, M. W. Beijersbergen, R. J. C. Spreeuw, and J. P. Woerdman, "Orbital angular momentum of light and the transformation of Laguerre-Gaussian laser modes," Phys. Rev. A **45**, 8185–8190 (1992).
13. M. Padgett, "Light's twist," Proc. Royal Soc. A: Math. Phys. Eng. Sci. **470**, 20140633 (2014).
14. S. Golowich, "Asymptotic theory of strong spin–orbit coupling in optical fiber," Opt. Lett. **39**, 92–95 (2014).
15. P. Gregg, P. Kristensen, A. Rubano, S. Golowich, L. Marrucci, and S. Ramachandran, "Spin-Orbit Coupled, Non-Integer OAM Fibers: Unlocking a New Eigenbasis for Transmitting 24 Uncoupled Modes," in *Conference on Lasers and Electro-Optics,* (OSA, San Jose, California, 2016), p. JTh4C.7.
16. Z. Zhang, J. Gan, X. Heng, Y. Wu, Q. Li, Q. Qian, D. Chen, and Z. Yang, "Optical fiber design with orbital angular momentum light purity higher than 99.9%," Opt. Express **23**, 29331–29341 (2015).
17. L. Wang, A. Corsi, L. A. Rusch, and S. LaRochelle, "Investigation of orbital angular momentum mode purity in air-core optical fibers," in Photonics Society Summer Topical Meeting Series (SUM), (IEEE, 2016), pp. 203–204.
18. R. M. Nejad, L. Wang, J. Lin, S. LaRochelle, and L. A. Rusch, "The Impact of Modal Interactions on Receiver Complexity in OAM Fibers," J. Light. Technol. **35**, 4692–4699 (2017).
19. D. Marcuse, "Coupled-mode theory for anisotropic optical waveguides," The Bell Syst. Tech. J. **54**, 985–995 (1975).
20. L. Palmieri, "Coupling mechanism in multimode fibers," in Photonics West, Proc. SPIE 9009, Next-Generation Optical Communication: Components, Sub-Systems, and Systems III, (2014), p. 90090G.
21. C. Antonelli, A. Mecozzi, M. Shtaif, and P. J. Winzer, "Stokes-space analysis of modal dispersion in fibers with multiple mode transmission," Opt. Express **20**, 11718–11733 (2012).
22. N. Imoto, N. Yoshizawa, J. Sakai, and H. Tsuchiya, "Birefringence in single-mode optical fiber due to elliptical core deformation and stress anisotropy," IEEE J. Quantum Electron. **16**, 1267–1271 (1980).
23. D. Chowdhury and D. Wilcox, "Comparison between optical fiber birefringence induced by stress anisotropy and geometric deformation," IEEE J. Sel. Top. Quantum Electron. **6**, 227–232 (2000).
24. P. K. A. Wai and C. R. Menyuk, "Polarization mode dispersion, decorrelation, and diffusion in optical fibers with randomly varying birefringence," J. Light. Technol. **14**, 148–157 (1996).
25. L. Wang, P. Vaity, S. Chatigny, Y. Messaddeq, L. A. Rusch, and S. LaRochelle, "Orbital-Angular-Momentum Polarization Mode Dispersion in Optical Fibers," J. Light. Technol. **34**, 1661–1671 (2016).
26. J. P. Gordon and H. Kogelnik, "PMD fundamentals: Polarization mode dispersion in optical fibers," PNAS **97**, 4541–4550 (2000).
27. K. P. Ho and J. M. Kahn, "Linear Propagation Effects in Mode-Division Multiplexing Systems," J. Light. Technol. **32**, 614–628 (2014).
28. L. Palmieri and A. Galtarossa, "Intramodal Dispersion Properties of Step-Index Few-Mode Spun Fibers," J. Light. Technol. **34**, 303–313 (2016).
29. A. Galtarossa, L. Palmieri, M. Schiano, and T. Tambosso, "Measurement of birefringence correlation length in long, single-mode fibers," Opt. Lett. **26**, 962–964 (2001).
30. P. K. A. Wai and C. R. Menyuk, "Polarization decorrelation in optical fibers with randomly varying birefringence," Opt. Lett. **19**, 1517–1519 (1994).

Optics EXPRESS

31. D. Marcuse, "Derivation of coupled power equations," The Bell Syst. Tech. J. **51**, 229–237 (1972).
32. K. Saitoh and S. Matsuo, "Multicore Fiber Technology," J. Light. Technol. **34**, 55–66 (2016).
33. P. J. Winzer, A. H. Gnauck, A. Konczykowska, F. Jorge, and J. Dupuy, "Penalties from in-band crosstalk for advanced optical modulation formats," in 37th European Conference and Exhibition on Optical Communication, (2011), pp. 1–3.
34. J. Proakis, *Digital Communications*, McGraw-Hill series in electrical and computer engineering : communications and signal processing (McGraw-Hill, 2007).
35. A. Mecozzi, C. Antonelli, and M. Shtaif, "Nonlinear propagation in multi-mode fibers in the strong coupling regime," Opt. Express **20**, 11673–11678 (2012).
36. A. Mecozzi, C. Antonelli, and M. Shtaif, "Coupled Manakov equations in multimode fibers with strongly coupled groups of modes," Opt. Express **20**, 23436–23441 (2012).